Abdominal Radiology (2023) 48:2207–2218
https://doi.org/10.1007/s00261-023-03920-2

HOLLOW ORGAN GI

Application of intravoxel incoherent motion diffusion-weighted imaging for preoperative knowledge of lymphovascular invasion in gastric cancer: a prospective study

Jing Li[1] · Liang-liang Yan[1] · Hong-kai Zhang[1] · Yi Wang[2] · Shu-ning Xu[3] · Xue-jun Chen[1] · Jin-rong Qu[1]

Received: 24 February 2023 / Revised: 9 April 2023 / Accepted: 11 April 2023 / Published online: 21 April 2023

Abstract

Purpose To investigate the potential of intravoxel incoherent motion diffusion-weighted imaging (IVIM) for preoperative prediction of lymphovascular invasion (LVI) in gastric cancer (GC).

Methods This study prospectively enrolled 90 patients (62 males, 28 females, 60.79 ± 9.99 years old) who received radical gastrostomy. Abdominal MRI examinations including IVIM were performed within 1 week before surgery. Patients were divided into LVI-positive and -negative group according to pathological diagnosis after surgery. The apparent diffusion coefficient (ADC) and IVIM parameters, including true diffusion coefficient (*D*), pseudodiffusion coefficient (*D**), and pseudodiffusion fraction (*f*), were compared between the two groups. The relationship between MRI parameters and LVI was studied by Spearman's correlation analysis. Multivariable logistic regression analysis was used to screen independent predictors of LVI. Receiver-operating characteristic curve analyses were applied to evaluate the efficacy.

Results The ADC, *D* in LVI-positive group were lower, whereas tumor thickness and *f* parameter in LVI-positive group were higher than those in LVI-negative group, and they were statistically correlated with LVI ($p < 0.05$). *D*, *f* and tumor thickness were independent risk factors of LVI. The area under the curve of ADC, *D*, *f*, thickness, and the combined parameter ($D + f$ + thickness) were 0.667, 0.754, 0.695, 0.792, and 0.876, respectively. The combined parameter demonstrated higher efficacy than any other parameters ($p < 0.05$).

Conclusion The ADC, *D*, and *f* can effectively distinguish LVI status of GC. The *D*, *f* and thickness were independent predictors. The combination of the three predictors further improved the efficacy.

Keywords Diffusion magnetic resonance imaging · Stomach neoplasms · Lymphovascular invasion

✉ Jin-rong Qu
qjryq@126.com

Jing Li
lijingqingqing@163.com

Liang-liang Yan
yanliangliang2008@126.com

Hong-kai Zhang
zhk625@sina.com

Yi Wang
wyft1022@163.com

Shu-ning Xu
lindaxsn1985@163.com

Xue-jun Chen
chenxuejun1967@163.com

[1] Department of Radiology, The Affiliated Cancer Hospital of Zhengzhou University (Henan Cancer Hospital), No. 127, Dongming Road, Zhengzhou 450008, Henan, China

[2] Department of Pathology, The Affiliated Cancer Hospital of Zhengzhou University (Henan Cancer Hospital), No.127, Dongming Road, Zhengzhou 450008, Henan, China

[3] Department of Digestive Oncology, The Affiliated Cancer Hospital of Zhengzhou University (Henan Cancer Hospital), No.127, Dongming Road, Zhengzhou 450008, Henan, China

Introduction

Despite the incidence of gastric cancer (GC) has been decreasing over the past decade, it still ranks third for the mortality globally [1], and remains the third most common cancer in China [2]. The optimal treatment for GC strongly relies on accurate clinical staging, however, the discordance rate of clinical and pathologic staging is up to 65.6% [3], causing a misguidance of treatment and prognosis prediction. Surgical resection is the standard procedure for treating GC, but the local recurrence after surgery remains high [4]. The American Joint Committee on Cancer (AJCC) tumor-node-metastasis (TNM) staging system has established the guidance for treatment allocation and prognostic prediction on GC; however, it failed to distinguish individual survival among patients in the same stage [5]. Recent studies have addressed the close relationship between lymphovascular invasion (LVI) and recurrence and prognosis among different GC populations [6, 7]. Choi et al. and Lu et al. have suggested the incorporation of LVI into the TNM system for more accurate staging and risk stratification [8, 9]. Hence, the preoperative knowledge of LVI becomes urgently desirable and would facilitate individualized medical care for GC.

LVI regards to tumour cells invading into lymphatic and/or blood vessel near tumor, and is responsible for tumor aggressiveness and locoregional dissemination [10]. Despite the progonostic significance of LVI [6–9], it can only be diagnosed on surgical specimens, which limits its use for early prediction. Therefore, it is necessary to establish a reliable LVI-related predictor preoperatively. Meng et al. [11] have developed a clinical model for preoperative assessment of LVI, but ignored imaging data, which is the basic standard of care in practice. Ma et al. [12] has addressed the potential of multiphasic enhanced CT in evaluating LVI. However, concerns such as radiation, lacking functional information, and low soft tissue contrast in CT have led to increased use of magnetic resonance imaging (MRI) for characterisation of GC [4, 13].

Emerging CT-based radiomics and deep learning algorithm have been applied to develop models for the prediction of LVI [14, 15], but this method suffer from the lack of simplicity, reproducibility, repeatability, and way from utility in real-world practice. Functional MRI opens up the possibility of quantifying tumor characteristics and provides more information [4, 13], for example, DWI improves T and N staging in GC [16], but the related apparent diffusion coefficient (ADC) parameter is derived from a simple mono-exponential model in which the diffusion displacements are assumed to follow a Gaussian distribution, which is not the case in heterogeneous biological tissues like cancer [17]. Therefore, additional noninvasive quantitative methods are needed to better character tumor heterogeneity. Intravoxel incoherent motion (IVIM) has roots in DWI; it separates and quantifies pure water molecular diffusion and microcirculatory perfusion through three parameters calculated by the bi-exponential model: true diffusion coefficient (D), pseudodiffusion coefficient (D^*), and pseudodiffusion fraction (f) [18]. Collectively, these parameters offer a multi-faceted characterization of cancerous tissues. The IVIM sequence has been increasingly employed to characterize tumor heterogeneity in several cancers [19–21]. Regarding GC, IVIM has been applied for better staging in a clinical study [22] and evaluating treatment response in a mice experiment [23]. Together with DCE, IVIM is potentially useful for assessing pathologic response to NAC [24]. These studies clearly underline the feasibility of using IVIM for GC. However, whether IVIM can serve as a reliable marker for noninvasive evaluation for LVI has not been well-established. We hypothesize that since IVIM derives multiple parameters that reflect more comprehensive information of tumor, it may potentially predict LVI.

Therefore, we conduct this prospective work to identify significant LVI-related IVIM parameters and the potential of IVIM as an imaging-based assessment of LVI in resectable GC.

Methods

Study population

This prospective study was approved by the institutional review board of our hospital. Informed consent was obtained from each patient (NCT04028375). Consecutive GC patients between January 2021 and Dec 2022 were prospectively recruited. The inclusion criteria: (1) endoscopy biopsy confirmed as gastric adenocarcinomas; (2) GC lesions were evaluated as resectable (cT1–4a/N0–1/M0) by a multidisciplinary team (MDT) and referred to surgery; (3) patients underwent MRI examination including IVIM and DWI. The exclusion criteria were: (1) pathologically confirmed as mixed adenocarcinomas after surgery; (2) accept neoadjuvant treatment prior to surgery; (3) poor image quality due to severe artifacts and distortion, causing unsuccessful tumor identification and measurement (image quality score > 3 with a 4-point scale method scored by two radiologist simultaneously); (4) the maximal diameter of tumor is less than 10 mm, insufficient to place a valid region of interest (ROI). The recruitment process is displayed in Fig. 1. Besides, The MDT, as part of the standard care procedure in our hospital, consisted of specialists in gastrointestinal surgery, digestive oncology, radiotherapy oncology, radiology, pathology and endoscopy. Clinical staging and surgical resectability of each

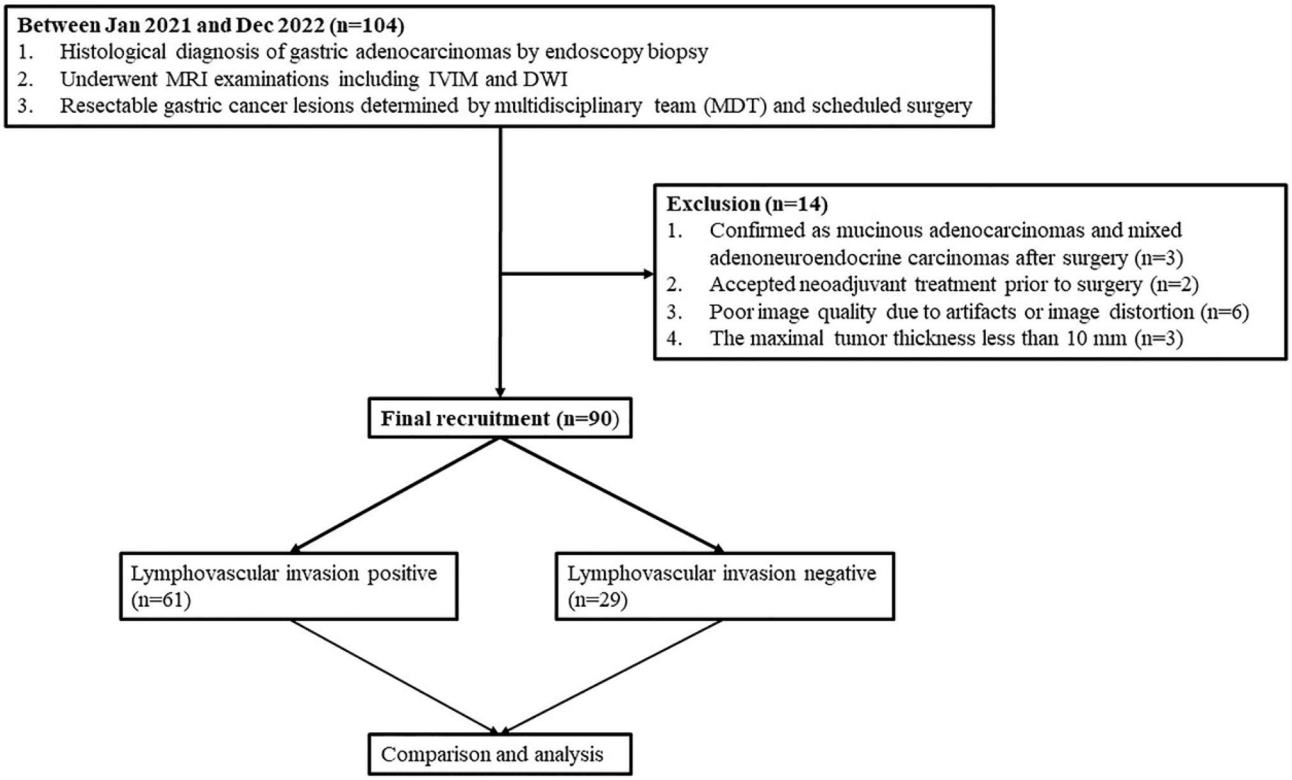

Fig. 1 Flowchart of patient's recruitment

tumor were determined by interpretating preoperative imaging data and the optimal treatment plan was made after the careful and comprehensive review and assessment of patient history, imaging, laboratory information, and patient status (e.g., if active bleeding, obstruction, or severe anemia was presented).

MRI protocol

IVIM-MRI scans were performed within 1 week (median: 3 days) before surgery on a 3.0 T MR platform (Magnetom Prisma, Siemens Healthineers) with an anterior 18-element body coil and in-built posterior 32-element spine coil array. The pre-examination preparation included: (1) Patients fasted for 12 h, (2) Respiration training for slow and rhythmic breath in order to reduce unwanted artifacts, (3) Stomach distention by drinking 800 mL of warm water 10 min before acquisition, (4) Reduction of gastric peristalsis by intramuscular administration of raceanisodamine hydrochloride injection (10 mg, Ningbo Dahongying Pharmaceutical Co.). The standard protocol, as listed in Table 1, included (1) 3D volumetric interpolated breath-hold examination (VIBE) opp-in axial T_1WI, (2) axial respiratory triggered, fat-suppressed turbo spin echo (fs_TSE) T2WI, and (3) IVIM acquired using a prototyped integrated specific slice dynamic Shim (iShim) sequence. This sequence first acquires 2D multi-gradient echo images for each imaging slice with its FOV and orientation adapted from the respective imaging slice. The difference in the echo time between the first and last echoes was selected such that fat and water alias. Next, a phase difference image was calculated from these two echoes. The accuracy of D^* calculation requires more than 4 b value range from 0 to 200 s/mm^2 [25], and higher b value is recommended for better tumor detection and comparison [22, 23, 26]. Twelve b values (0, 25, 50, 75, 100, 200, 400, 600, 800, 1000, 1200, and 1600 s/mm^2) were applied [27]. The total acquisition time of T1WI, T2WI, and IVIM was 16 s, 2:40–4:30 min, and 3:40 min, respectively. 3D Diagonal diffuse mode was used and the parameter of G (the diffusion gradient amplitude) was 80 mT/m, δ (the diffusion gradient duration) was 11.1 ms, Δ (the time between the leading edges of the diffusion gradient pulses) was 23.9 ms.

Image interpretation

The IVIM raw data were processed using the MADC software in FuncTool software package. Two radiologists with 12 and 14 years of experience in gastrointestinal (GI) radiology reviewed the images and measured IVIM parameters in a dual-blind manner. The image quality was

Table 1 MRI standard protocol

Parameters	T1WI axial	T2WI axial	IVIM (b = 0, 25, 50, 75, 100, 200, 400, 600, 800, 1000, 1200, 1600 s/mm^2)
TR (ms)	3.9	4500–7800	8000
TE (ms)	1.32/2.74	98	59
Slice thickness (mm)	5	5	5
Slice gap (mm)	NA	0.5	0.5
NEX	1	2	1–4
FOV (cm^2)	38 × 38	28.7 × 28.7	38 × 38
Resolution	180 × 288	193 × 384	83 × 128
Voxel size (mm^3)	1.47 × 1.32 × 4.23	1.49 × 1.04 × 5	3.28 × 2.665
Flip angle(°)	9	120	NA

NEX for IVIM range from 1 to 4, NEX = 1 for b = 0, 25, 50, 75, 100, 200, 400 s/mm^2, NEX = 2 for b = 600, 800 s/mm^2, NEX = 3 for b = 1000 s/mm^2, NEX = 4 for b = 1200, 1600 s/mm^2

TR repetition time, *TE* echo time, *NEX* number of excitations, *FOV* field of view

scored using a 4-point scale method, point 1 represents no artifacts or image distortion; 2, mild; 3, moderate; 4, severe. Images with scores equal 4 by the two radiologist consistently were excluded. For IVIM parameter measurements, taking T2WI and IVIM-DWI with b = 800 s/mm^2 as reference, the readers manually draw a freehand ROI along the outer contour of the GC lesion on the maximal axial plane. The ADC from mono-exponential model was calculated following the formula: $Sb/S0 = \exp(-b \times ADC)$, where S0 repeasents signal intensity at b = 0 and Sb is the signal intensity at higher b values [18]. IVIM parameters was calculated with equation: $Sb/S0 = (1-f) \times \exp(-bD) + f \times \exp[-b(D+D^*)]$ [18]. A segmented fitting algorithm was used to fit IVIM [28, 29]. D was firstly estimated using b value above a threshold based on a linear fitting with ignoring perfusion compartment; then, f was calculated by comparing measured b = 0 signal and extrapolated b = 0 signal, based on the acquired D in first step by the conventional Mono-exponential model; and D^* could be fitted using a linear form by fixing the D and f in IVIM model. The b value threshold was 200 for the fitting [30]. Quantitative data were averaged after independent measurements by the two readers.

Morphologic parameters were recorded. Tumor thickness was determined by the maximal diameter vertical to the longest axis plane of the tumor. MRI reported serosal invasion (MRI reported cT4a) was assessed as positive when opacity or nodular infiltration in perigastric fatty plane was presented [16, 22]; MRI reported LN status: regional LN with maximal short diameter > 10 mm with or without heterogeneous enhancement, and/or clusters containing ≧ 3 lymph nodes, represents positive [16, 22]. Qualitative features were evaluated separately, if there was a divergence between the two readers for classification of any features, a third senior reader (19 years of experience) was introduced to reach a final diagnosis.

Pathologic LVI diagnosis

The surgical specimens were analyzed with hematoxylin and eosin (HE)-stained 4 μm thick section by a qualified GI pathologists with 12 years of experience, who was blind to MRI data. LVI positivity was reported when tumour emboli within either the lymphatic or vascular channels was presented [31]. Other recorded indicators included: pathologic tumor (pT) staging, lymph node metastasis (LNM) according the 8th AJCC criteria [5], perineural invasion (PNI), histodifferentiation, Lauren subtype, positive lymph node numbers (PLN), total dissected lymph node numbers (TLN). The positive lymph node ratios (PLNR) is the percentage ratio of PLN to TLN (PLNR = PLN/TLN × 100%).

Statistical analyses

SPSS23.0, and MedCalc software (version 18.0) were used for statistical analysis. The inter-observer agreement between readers was evaluated by the intraclass correlation coefficient (ICC) with a 95% confidence interval (CI) for quantitative variables and Kappa values for qualitative variables. The ICC/Kappa between 0.00 and 0.20 was defined as poor correlation; 0.21–0.40, fair; 0.41–0.60, moderate; 0.61–0.80, good; and 0.81–1.00, excellent. The Kolmogorov–Smirnov test was used to check the normality assumption, data consistent with the normality assumption was presented with mean ± standard deviation ($\bar{x} \pm s$), and skewness distributed data were described in median (25% quartile, 75% quartile) [M (Q1, Q3)] form. Univariate analysis was performed by Student's t test or Mann–Whitney U test. Categorical data were compared using the chi-square test or Fisher's exact test. Multivariable logistic regression was performed to screen independent predictors of LVI. Significant variables were further processed using the receiver operating characteristic (ROC) curve analysis to calculate the cut-off

thresholds. Specificity, sensitivity, the area under the curve (AUC), positive predictive value (PPV), and negative predictive (NPV) values were computed. The Delong test was used to compare the differences among AUCs. Correlations between IVIM parameters and LVI were assessed by Spearman's rank correlation test.

Results

Patient recruitment and clinicopathological characteristics

Among 104 consecutive patients, 14 were excluded, including 1 pathologically diagnosed mucinous adenocarcinomas and 2 mixed adenoneuroendocrine carcinomas after surgical resection, 2 received neoadjuvant chemotherapy before surgery, 6 had poor image quality (score = 4); 3 had small lesions with diameter under 10 mm assessed by the two radiologist simultaneously, which were insufficient to reach perfect tumor identification and reproducible free hand ROIs placement and valid ADC measurements. Thereafter, 90 were eventually recruited (58 males, 27 females), aged 60.79 ± 9.99 (39–81) years (Fig. 1). After surgery, 61 were LVI-positive (67.78%), 29 were LVI negative. As shown in Table 2, there were no statistical differences in age, sex, location, and TLN between LVI-positive and -negative groups ($p > 0.05$). There were significant differences of histodifferentiation, pT, LNM, PLN, PLNR, PNI, and Lauren subtype between the two groups ($p < 0.05$); specifically, the LVI-positive group had more cancers with poor differentiation, advanced pT3–4a (37 v.s 14), positive LNM (55 v.s 4) and PNI (43 v.s 8), higher PLN and PLNR, and diffused Lauren subtype (36 v.s 12).

Table 2 Clinicopathological characteristics of patients in LVI-positive and -negative group

Characteristics		LVI negative ($n = 29$)	LVI-positive ($n = 61$)	$t/Z/\chi^2$ value	p value
Age (years)	Range: 39–81, average: 60.79 ± 9.99	57.97 ± 9.08	62.13 ± 9.94	1.874[a]	0.064
Sex	Male	20	42	< 0.001[b]	0.991
	Female	9	19		
Location	Cardia/Fundus	11	24	0.778[b]	0.678
	Body	10	25		
	Antrum	8	12		
pT staging	1	0	2	–	< 0.001
	2	13	3		
	3	8	10		
	4a	6	27		
LNM	Negative	25	6	51.577[b]	< 0.001
	Positive	4	55		
PLN	Range: 0–54	0 (0, 0.5)*1	6 (1, 11)*2	5.396[c]	< 0.001
TLN	Range: 15–70	22 (17, 31.5) Δ1	26 (20, 35.5) Δ2	1.448[c]	0.148
PLNR (%)	Range: 0–86.21	0 (0, 0)#1	19.64 (5, 40.55)#2	6.683[c]	< 0.001
Histodifferentiation	Poor	13	43	13.031[b]	0.001
	Moderate	11	18		
	Well	5	0		
Perineural invasion	Negative	21	18	14.735[b]	< 0.001
	Positive	8	43		
Lauren subtype	Intestinal	12	9	7.799[b]	0.020
	Mixed	5	16		
	Diffused	12	36		

PLN, TLN, PLNR are displayed in *M (Q1, Q3)* form. Upper "a" in the fifth column represents using student *t* test for comparison; "b": using $\chi 2$ test; "c": using Mann–Whitney *U* test; "–" means using Fisher's exact test, and there is no definite statistical value

LVI lymphovascular invasion, *PNI* perineural invasion, *PLN* positive lymph node numbers, **1* range of 0–32 in LVI-negative group, **2* range of 0–54 in LVI-positive group, *TLN* total dissected lymph node numbers in surgery; *Δ1* range 15–48 in LVI-negative group, *Δ2* range of 18–70 in LVI-positive group, *PLNR* positive lymph node ratio, ratio of positive lymph nodes to the total dissected lymph nodes, *#1* range of 0–10.71% in LVI-negative group, *#2* range of 0–86.21% LVI-positive group

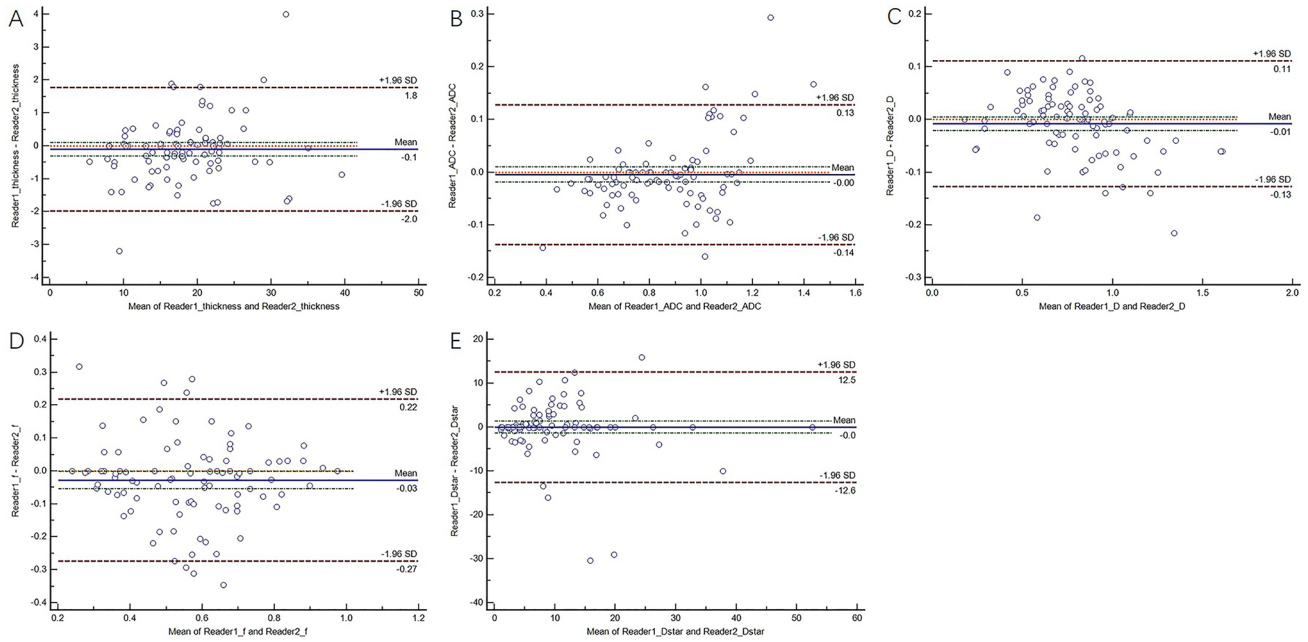

Fig. 2 Bland–Altman plot diagrams for inter-observer agreement of quantitative parameters measurements between the two readers. **A** ICC for tumor thickness; **B** ICC for ADC; **C** ICC for *D*; **D** ICC for *D**; **E** ICC for *f*

Interobserver agreement

The inter-observer agreement between the readers' assessment was good or excellent (Fig. 2). The kappa value for image quality score was 0.921 (95%, 0.834–1), and the ICC values for ADC, *D*, *D**, *f*, and tumor thickness measurements was 0.973 (0.959–0.982), 0.982 (0.972–0.988), 0.856 (0.781–0.905), 0.864 (0.794–0.911), 0.989 (0.984–0.992), separately.

MRI parameters

GC lesions no matter with or without LVI, were hyperintense on DWI and hypointense on ADC map (Figs. 3, 4A, B). The overall tumor thickness was 18.23 ± 6.61 (range 10–43.12) mm. Tumor thickness in LVI-positive group (Fig. 3) was statistically higher than that in LVI-negative group (Fig. 4). The mean value of ADC, *D* in LVI-positive group was statistically lower, whereas the mean value of *f* was higher compared to LVI-negative group ($p < 0.05$). Furthermore, there were significant differences of MRI reported serosal invasion and LN status between the two groups ($p < 0.05$); specifically, LVI-positive group contains more patients in higher clinical stage of positive MRI reported serosal invasion (15 v.s 1) and LN status (31 v.s 6). Although the mean value of *D** in LVI-positive group was slightly higher than that in LVI-negative group, the difference showed no statistical significance ($p = 0.237$, Table 3).

The predictive efficacy of IVIM parameters

Significant LVI-related parameters determined by univariable analysis included ADC, *D*, *f*, MRI reported serosal invasion, MRI reported LN status, and tumor thickness; thereafter, they were analyzed through multiple logistic regression analysis for further selection of independent risk factors of LVI. The results revealed that taking $D \leq 0.85 \times 10^{-3}$mm^2/s (odds ratio [OR], 95% CI 1.105 [1.000–3.977]), $f > 0.51$ (397.022 [5.461–3606.39]), and tumor thickness > 15.00 mm (1.253 [1.095–1.434]) as cut-off values, they were independent risk factors of LVI ($p = 0.013$, 0.007, 0.001, Table 4) and were used to build a combined parameter (*D* + *f* + thickness). Additionally, Hosmer and Lemeshow test revealed good consistency between the predicted probability of LVI by the combined parameter and the actual probability ($\chi^2 = 5.084$, $p = 0.749$).

ROC analyses revealed that the combined parameter yielded the highest AUC of 0.876 for distinguishing LVI positivity, followed by thickness, D, *f*, and ADC with AUC achieving 0.792, 0.754, 0.695, and 0.667, respectively (Fig. 5, Table 5). The combined parameter showed statistically higher efficacy than thickness, *D*, *f*, and ADC (Delong test, $Z = 2.633$, 2.291, 2.979, 2.675, $p = 0.009$, 0.022, 0.003, 0.008); however, no significant differences were observed among AUCs yielded by single parameters (all $p > 0.05$). Furthermore, the morphologic parameters, MRI reported serosal invasion and MRI reported LN status, yielded AUCs of 0.606 (0.497–0.707), 0.651 (0.543–0.748), statistically

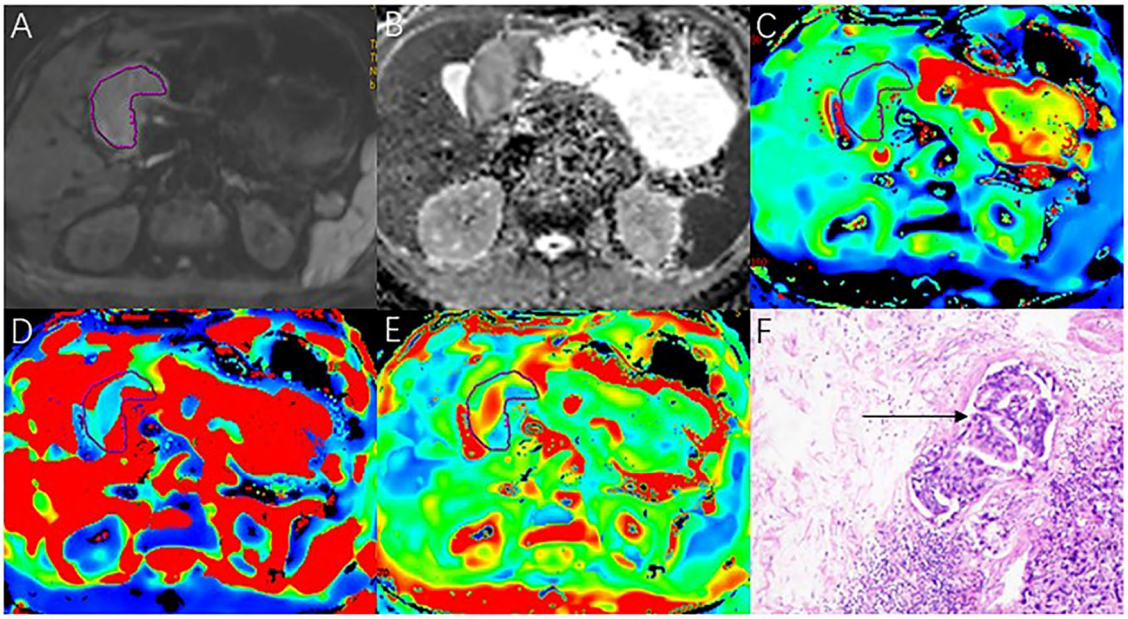

Fig. 3 IVIM maps of a lymphovascular invasion (LVI) positive case. Male, 68 years old, surgical-pathologically confirmed gastric adenocarcinoma in gastric antrum, staging of pT3N3aM0, tumour thickness was 34.85 mm. **A** A freehand ROI (red contour) was manually delineated along the margin of tumor (hyperintense) on reference image of DWI with $b = 800$ s/mm^2. **B–E** The corresponding ADC, D, D*, and f maps showed the ADC value was 0.935×10^{-3} mm^2/s, D value was 0.922×10^{-3} mm^2/s, D* value was 3.837×10^{-3} mm^2/s, and f value was 0.638. **F** The histopathology (HE, magnification: × 200) demonstrated lymphovascular space was filled with numerous adenocarcinomas cells (black arrow)

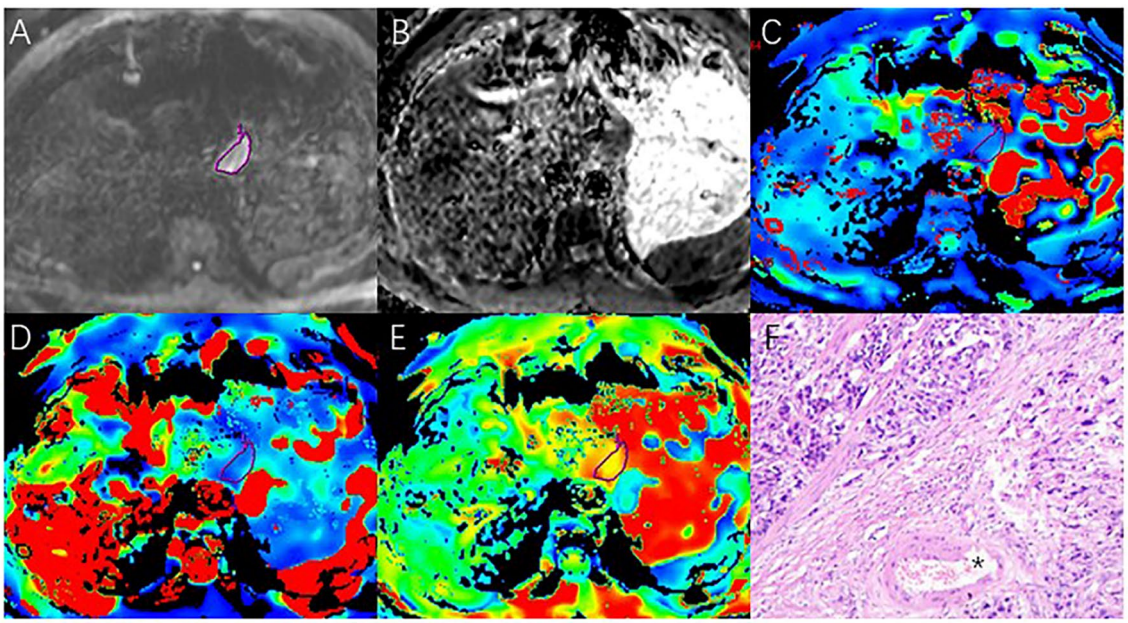

Fig. 4 IVIM maps in a lymphovascular invasion (LVI)-negative case. Male, 69 years old, surgical-pathologically confirmed gastric adenocarcinoma in gastric cardia, staging of pT2N0M0, tumour thickness was 12.45 mm. **A** A freehand ROI (red contour) was manually delineated along the margin of tumor (hyperintense) on reference image of DWI with $b = 800$ s/mm^2. **B–E** The corresponding ADC, D, D*, and f maps showed the ADC value was 0.957×10^{-3} mm^2/s, D value was 0.895×10^{-3} mm^2/s, D* value was 4.447×10^{-3} mm^2/s, and f value was 0.585 of the tumor. **F** The histopathology (HE, magnification: × 200) demonstrated normal lymphovascular structure (*)

Table 3 Comparison of MRI parameters between LVI-positive and LVI-negative groups

Parameters		LVI negative ($n = 29$)	LVI-positive ($n = 61$)	$t/Z/\chi^2$ value	p value
Thickness	Mean: 18.23 ± 6.61 Range: 10–43.12	13.64 ± 5.23	20.41 ± 6.08	5.156	< 0.001
MRI reported LN status	Negative	23	30	7.370	0.007
	Positive	6	31		
MRI reported serosal invasion	Negative	28	46	6.010	0.014
	Positive	1	15		
ADC ($\times 10^{-3}$ mm^2/s)		0.99 ± 0.23	0.88 ± 0.19	− 2.252	0.031
D ($\times 10^{-3}$ mm^2/s)		0.92 ± 0.33	0.78 ± 0.22	− 3.293	0.023
D^* ($\times 10^{-3}$ mm^2/s)		7.40 (5.83, 15.65)	6.72(3.32, 12.05)	− 1.183	0.237
f		0.47 ± 0.14	0.55 ± 0.14	2.228	0.028

LVI lymphovascular invasion, *ADC* apparent diffusion coefficient, *D* true diffusion coefficient, *D** Pseudodiffusion coefficient, *f* pseudodiffusion fraction; *D** is displayed in *M* (*Q*1, *Q*3) form

Table 4 Predictive MRI parameters for the prediction of PNI status

Variables	β	Standard error	Wald	Odds ratio (95% CI)	p value
D ($\times 10^{-3}$mm^2/s)	4.200	1.685	6.213	1.105 (1.000–3.977)	0.015
f	5.984	2.213	7.288	397.022 (5.461–3606.39)	0.007
Tumor thickness	0.226	0.069	10.859	1.253 (1.095–1.434)	0.001

D true diffusion coefficient, *f* pseudodiffusion fraction

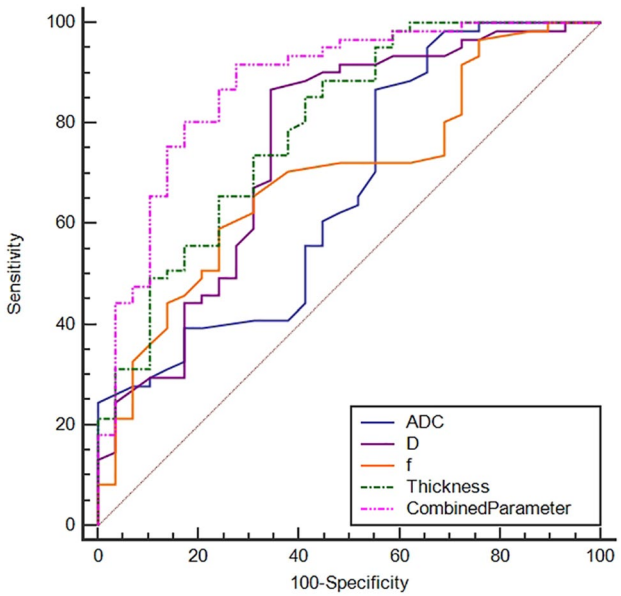

Fig. 5 ROC analysis of ADC, *D*, *f*, thickness and the combined parameter ($D + f +$ thickness) in differentiating lymphovascular invasion status

lower than AUC of the combined parameter ($Z = 6.383$, 4.357, $p < 0.001$) and thickness ($Z = 3.570$, 2.174, $p = 0.005$, 0.03).

Negative correlations were identified between ADC, *D* and LVI ($r = -0.418$, -0.303; $p = 0.003$, 0.027); whereas thickness, *f* and the combined parameter showed positive correlations with LVI ($r = 0.473$, 0.233, 0.608; $p < 0.001$).

Discussion

This prospective work preliminarily explored the potential of functional IVIM sequence for preoperative knowledge of LVI status in resectable GC. The ADC, *D*, *f*, and tumor thickness are effective markers for the discrimination of LVI. The *D*, *f*, and tumor thickness were independent predictors of LVI and their combination further improved the predictive capability.

LVI positivity in GC has been reported to be 13.1–74.8%, varies among different disease stages; overall, the likelihood of LVI increases in advanced GC [6–8, 12, 14, 15], and LVI is closely associated with tumor size, *T* staging, and LNM [6–8]; similarly, we found significant differences in tumor thickness, pT, LNM between LVI-positive and -negative groups, suggesting larger and advanced GC tend to present positive LVI. Moreover, ADC and *D* were negatively correlated with cellular density, and lower ADC indicated poor differentiation and high TNM staging in GC [22, 32]. LVI positivity represents tumor cells infiltrating into the lymphovascular channels, a process theoretically would lead to increasement of tumor cells and the narrowing of the intercellular spaces, consequently causing a reduced ADC and *D* value [18]. Liu et al. [16] has found conventional ADC is

Table 5 Diagnostic efficacy of MRI quantitative parameters for the prediction of LVI status

Parameters	AUC (95% CI)	Sensitivity (%)	Specificity (%)	PPV (%)	NPV (%)	Youden index	Cut off value	*Z* value	*p* value
ADC ($\times 10^{-3}$mm^2/s)	0.667 (0.560–0.763)	86.89	44.83	76.82 (65.10–786.13)	61.91 (38.44–81.90)	0.317	0.97	2.633	0.009
D ($\times 10^{-3}$mm^2/s)	0.754 (0.651–0.838)	86.89	65.52	84.13 (72.74–92.12)	70.38 (49.82–86.25)	0.524	0.85	4.298	< 0.001
f	0.695 (0.589–0.788)	59.02	75.86	83.72 (69.30–93.20)	46.81 (32.11–61.92)	0.349	0.51	3.348	0.001
Thickness	0.792 (0.694–0.871)	85.25	58.62	81.25 (69.54–89.92)	65.39 (44.34–82.79)	0.439	15.00	5.638	< 0.001
Combined parameter (*D* + *f* + thickness)	0.876 (0.789–0.936)	91.80	72.41	87.50 (76.85–94.45)	80.76 (60.64–93.44)	0.642	0.52	9.016	< 0.001

LVI lymphovascular invasion, *AUC* area under the curve, *ADC* apparent diffusion coefficient, *D* true diffusion coefficient, *D** pseudodiffusion coefficient, *f* pseudodiffusion fraction, *CI* confidence interval, *PPV* positive predictive value, *NPV*-negative predictive value

effective in differentiating pT2 vs. pT3, pT3 v.s pT4, pN0 v.s pN+, however, their study is small sized and they did not screen specific imaging-based risk factors for staging; additionally, conventional ADC is calculated using the mono-exponential diffusion model, assuming ideal Brownian diffusion condition which is not the case in cancerous tissue [17]. When comparing the capability between ADC and *D*, *D* has overweighed ADC, a consistent finding with previous studies [19–22]. Song et al. [23] has explored the potential of IVIM in monitoring treatment response to chemotherapy based on mice models, they found that ADC and *D* were positively correlated with intratumoral necrosis and cellular apoptosis, thus reflect the true molecular diffusion; their study is novel but data acquired not from humanbeings, which may mitigate its clinical use in practice. However, Zeng et al. [22] apllied IVIM for TN staging in GC, their results showed that *D* was the only useful parameter. The current studies on IVIM application in GC yields conflicting results, the underlying reasons may include that they used different *b* values for IVIM acquisition on variety of MRI ventors, focused on different clinical problems, as well as disparate patient cohorts. Differently, we applied the prototyped integrated specific slice dynamic Shim (iShim) sequence for IVIM acquisition; iShim has been increasingly employed in abdominal MRI to reduce geometric deformation and improve image quality [33]. The image quality and the inter-observer reproducibility of IVIM parameter measurement were good in this study, indicating the feasibility of using iShim technique for IVIM acquisition on stomach. Furthermore, we analyzed morphologic features together to build a combined parameter, which can be used for individual prediction of LVI in GC patients by using the cut-off values.

The applicative potential of *D** in tumor characterization and staging differs remarkably among cancers with conflicting results [21, 22, 34]. In terms of GC, current results are disappointing, for instance, according to Zeng et al.'s investigation, *D** was not useful for *T* and *N* staging [22]; Zhu et al. found that *D** showed no significant potential in predicting treatment response to NAC [24]. In this study, we found no significant difference of *D** between different LVI status, meaning that *D** is not capable for preoperative knowledge of LVI. One possible reason may due to the limited sample size of this preliminary study. Another underlying reason could be that *D** is vulnerable to noise and the selection of lower *b* values (< 200 s/mm^2) [30, 35], the stability and reproducibility of measuring *D** remains the lowest among IVIM parameters [36]. The other factors that may be responsible for calculation of *D** included: Bi-exponential fitting problems; numbers and magnitude of *b* values [36, 37]. Summationally, the prospect of D* utilization in real-world GC practice is unclear and needs more investigation.

Current IVIM explorations on GC have reported limited potential of *f* parameter [22, 24]. Differently, we found that *f* is significantly different between LVI-positive and negative group and is one of independent predictors of LVI, a preliminary but encouraging finding. The *f* reflects tumor microcirculation like the numbers of functional vessels, capillary network, and the permeability of the capillaries, etc. [35]. Destruction of lymphovascular structures may increase the microvascular permeability, which can account for a higher *f* value in LVI-positive group. However, the real molecular diffusion and microcirculation in vivo cancerous tissue is complicated, the ability of *f* for tumor characterization needs more studies to validate.

In this study, we not only analyze quantitative parameters of IVIM, but also interpreted the conventional morphologic features, which is the most common and fundamental imaging assessment for tumor [13]. Our results

revealed that tumor thickness overweighs other morphologic features and is a predictor of LVI, which is in accordance with previous CT studies [38, 39]. Tumor thickness represents the maximal depth of tumor infiltrating into the gastric wall, which is considered to be part of standard of care for cT staging [4, 16, 22, 38, 39]. As LVI is strongly related to T staging [9–12], tumor with larger thickness tend to have higher possibility of LVI, as our results suggested. Notely, MRI reported serosal invasion (equivalent to cT staging) was significant in univariate analysis, but was removed in multivariate analysis, partially because it is largely influenced by thickness. Therefore, tumor thickness may have more promising application prospect, because first, it presented good reproducibility with excellent ICC; second, compared to cT, it is quantitative and relatively less expertise dependent; third, its maximum accessibility on images allows the wide use in clinical routine.

Previous CT studies have demonstrated a better efficacy when combing quantitative parameters and qualitative features [38, 39]. IVIM is not the standard imaging modality for GC [4, 22, 35]; but IVIM together with morphologic MRI can provide complementary information. We found that incorporating thickness, D and *f*, outperformed any other parameters for predicting LVI, suggesting the superiority and usability of a combined imaging marker. Since LVI has been recommended to be added into TNM system for more accurate staging and prognosis evaluation [8, 9], the preoperative knowledge of LVI has certain clinical relevance. Accurate prediction of LVI by baseline IVIM-MRI would be beneficial for preoperative risk stratification and assist the management for GC.

There were several limitations in our study. First, the number of participants was relatively small, and this was a single-center study. Second, ROI delineation was completed on the maximal slice, which may introduce selection bias. Third, mucinous and mixed adenocarcinomas were excluded because they have more complicated histological components which could lead to variation of ADC values and affect the results of predictive analysis. Last, the *b* value sets for IVIM in GC lacks worldwide consensus. We applied the 12-*b* values sequence, which may not be the optimal or standard scanning specification for IVIM. Further studies with larger sample size from multiple centers are warranted.

In conclusion, our study demonstrated that IVIM is beneficial for preoperative knowledge of LVI in resectable GC; IVIM parameters together with tumor thickness provide additional information and further improve the efficacy. The combination of IVIM with other functional sequences like diffusion kurtosis imaging, DCE and multiparametric MRI-based radiomics are expected in future studies.

Author contributions Conceptualization: JL, JQ; Methodology: HZ, SX; Formal analysis and investigation: JL, LY, YW; Writing—original draft preparation: JL, YW; Writing—review and editing: JQ, XC; Funding acquisition: JL, JQ; Resources: JQ; Supervision: XC. All authors read and approved the final manuscript.

Funding This work was supported by [Henan Provincial Medical Science and Technology Project (SBGJ202003011)], [National Natural Science Foundation of China (Nos. 82202146, 82271979)], [Special funding of Henan Health Science and Technology Innovation Talent Project (Nos. YXKC2020011, YXKC2021054)].

Data availability The datasets used and analyzed during the current study are available from the corresponding author on reasonable request.

Declarations

Competing interests The authors did not receive support from any organization for the submitted work.

Ethical approval The study was approved by the institutional review board of the Affiliated Cancer Hospital of Zhengzhou University (Henan Cancer Hospital, Zhengzhou, China) in accordance with the Declaration of Helsinki. All methods were carried out in accordance with relevant guidelines and regulations.

Informed consent Written informed consent was obtained from all individual patients included in the study (NCT04028375).

References

1. Sung H, Ferlay J, Siegel RL et al. (2021) Global Cancer Statistics 2020: GLOBOCAN Estimates of Incidence and Mortality Worldwide for 36 Cancers in 185 Countries. CA Cancer J Clin 71:209-249. https://doi.org/10.3322/caac.21660.
2. Cao W, Chen HD, Yu YW et al. (2021) Changing profiles of cancer burden worldwide and in China: a secondary analysis of the global cancer statistics 2020. Chin Med J (Engl) 134:783-791. https://doi.org/10.1097/CM9.0000000000001474.
3. Papageorge MV, de Geus SWL, Zheng J et al. (2021) The Discordance of Clinical and Pathologic Staging in Locally Advanced Gastric Adenocarcinoma. J Gastrointest Surg 25:1363-1369. https://doi.org/10.1007/s11605-021-04993-4.
4. Smyth EC, Nilsson M, Grabsch HI et al. (2020) Gastric cancer. Lancet 396:635-648. https://doi.org/10.1016/S0140-6736(20)31288-5.
5. Amin MB, Greene FL, Edge SB et al. (2017) The eighth edition AJCC cancer staging manual: Continuing to build a bridge from a population-based to a more "personalized" approach to cancer staging. CA Cancer J Clin 67:93–99. https://doi.org/10.3322/caac.21388.
6. Fujita K, Kanda M, Ito S et al. (2020) Association between Lymphovascular Invasion and Recurrence in Patients with pT1N+ or pT2-3N0 Gastric Cancer: a Multi-institutional Dataset Analysis. J Gastric Cancer 20:41-49. https://doi.org/10.5230/jgc.2020.20.e3.
7. Choi S, Song JH, Lee S et al. (2021) Lymphovascular Invasion: Traditional but Vital and Sensible Prognostic Factor in Early Gastric Cancer. Ann Surg Oncol 28:8928-8935. https://doi.org/10.1245/s10434-021-10224-6.
8. Lu J, Dai Y, Xie JW et al. (2019) Combination of lymphovascular invasion and the AJCC TNM staging system improves prediction of prognosis in N0 stage gastric cancer: results from a

high-volume institution. BMC Cancer 19:216. https://doi.org/10.1186/s12885-019-5416-8.
9. Hirabayashi S, Kosugi S, Isobe Y et al. (2014) Development and external validation of a nomogram for overall survival after curative resection in serosa-negative, locally advanced gastric cancer. Ann Oncol 25:1179-1184. https://doi.org/10.1093/annonc/mdu125.
10. Padera TP, Kadambi A, di Tomaso E et al. (2002) Lymphatic metastasis in the absence of functional intratumor lymphatics. Science 296:1883–1886. https://doi.org/10.1126/science.1071420.
11. Meng Y, Huang X, Liu J et al. (2021) A Novel Nomogram for Individually Predicting of Vascular Invasion in Gastric Cancer. echnol Cancer Res Treat 20:15330338211004924. https://doi.org/10.1177/15330338211004924.
12. Ma Z, Liang C, Huang Y et al. (2017) Can lymphovascular invasion be predicted by preoperative multiphasic dynamic CT in patients with advanced gastric cancer? Eur Radiol 27:3383-3391. https://doi.org/10.1007/s00330-016-4695-6.
13. Zhang Y, Yu J. The role of MRI in the diagnosis and treatment of gastric cancer. Diagn Interv Radiol 2020;26(3):176-182.
14. Li Q, Feng QX, Qi L et al (2022) Prognostic aspects of lymphovascular invasion in localized gastric cancer: new insights into the radiomics and deep transfer learning from contrast-enhanced CT imaging. Abdom Radiol (NY) 47:496-507. https://doi.org/10.1007/s00261-021-03309-z.
15. Chen X, Yang Z, Yang J et al. (2020) Radiomics analysis of contrast-enhanced CT predicts lymphovascular invasion and disease outcome in gastric cancer: a preliminary study. Cancer Imaging 20 (1):24. https://doi.org/10.1186/s40644-020-00302-5.
16. Liu S, Wang H, Guan W et al. (2015) Preoperative apparent diffusion coefficient value of gastric cancer by diffusion-weighted imaging: Correlations with postoperative TNM staging. J Magn Reson Imaging 42:837-43. https://doi.org/10.1002/jmri.24841.
17. Le Bihan D (2013) Apparent diffusion coefficient and beyond: what diffusion MR imaging can tell us about tissue structure. Radiology 268:318–322. https://doi.org/10.1148/radiol.13130420.
18. Le Bihan D, Breton E, Lallemand D et al. (1988) Separation of diffusion and perfusion in intravoxel incoherent motion MR imaging. Radiology 168:497-505. https://doi.org/10.1148/radiology.168.2.3393671.
19. Sun J, Wu G, Shan F et al. (2019) The Value of IVIM DWI in Combination with Conventional MRI in Identifying the Residual Tumor After Cone Biopsy for Early Cervical Carcinoma. Acad Radiol 26:1040-1047. https://doi.org/10.1016/j.acra.2018.09.027.
20. Yu XP, Wen L, Hou J et al. (2016) Discrimination between Metastatic and Nonmetastatic Mesorectal Lymph Nodes in Rectal Cancer Using Intravoxel Incoherent Motion Diffusion-weighted Magnetic Resonance Imaging. Acad Radiol 23:479-485. https://doi.org/10.1016/j.acra.2015.12.013.
21. Klaassen R, Steins A, Gurney-Champion OJ et al. (2020) Pathological validation and prognostic potential of quantitative MRI in the characterization of pancreas cancer: preliminary experience. Mol Oncol 14:2176-2189. https://doi.org/10.1002/1878-0261.12688.
22. Zeng Q, Hong Y, Cheng J et al. (2021) Quantitative study of preoperative staging of gastric cancer using intravoxel incoherent motion diffusion-weighted imaging as a potential clinical index. Eur J Radiol 141:109627. https://doi.org/10.1016/j.ejrad.2021.109627.
23. Song XL, Kang HK, Jeong GW et al. (2016) Intravoxel incoherent motion diffusion-weighted imaging for monitoring chemotherapeutic efficacy in gastric cancer. World J Gastroenterol 22:5520-5531.
24. Zhu Y, Jiang Z, Wang B et al. (2022) Quantitative Dynamic-Enhanced MRI and Intravoxel Incoherent Motion Diffusion-Weighted Imaging for Prediction of the Pathological Response to Neoadjuvant Chemotherapy and the Prognosis in Locally Advanced Gastric Cancer. Front Oncol 12:841460. https://doi.org/10.3389/fonc.2022.841460.
25. Guiu B, Petit JM, Capitan V et al. (2012) Intravoxel incoherent motion diffusion-weighted imaging in nonalcoholic fatty liver disease: a 3.0-T MR study Hillon P, Krausé D, Cercueil JP.. Radiology 265:96-103. https://doi.org/10.1148/radiol.12112478.
26. Cohen AD, Schieke MC, Hohenwalter MD et al. (2015) The effect of low b-values on the intravoxel incoherent motion derived pseudodiffusion parameter in liver. Magn Reson Med 73:306-311. https://doi.org/10.1002/mrm.25109.
27. Koh DM, Collins DJ, Orton MR.(2011) Intravoxel incoherent motion in body diffusion-weighted MRI: reality and challenges. AJR Am J Roentgenol 196:1351-1361. https://doi.org/10.2214/AJR.10.5515.
28. Zhang MC, Li XH, Huang SY et al. (2019) IVIM with fractional perfusion as a novel biomarker for detecting and grading intestinal fibrosis in Crohn's disease. Eur Radiol 29:3069-3078. https://doi.org/10.1007/s00330-018-5848-6.
29. Lu B, Yang X, Xiao X et al. (2018) Intravoxel Incoherent Motion Diffusion-Weighted Imaging of Primary Rectal Carcinoma: Correlation with Histopathology. Med Sci Monit 24:2429-2436. https://doi.org/10.12659/msm.908574. 20
30. Jalnefjord O, Montelius M, Starck G et al. (2019) Optimization of b-value schemes for estimation of the diffusion coefficient and the perfusion fraction with segmented intravoxel incoherent motion model fitting. Magn Reson Med 82:1541-1552. https://doi.org/10.1002/mrm.27826.
31. Burgart LJ, Chopp WV, Jain D et al. (2021) Protocol for the Examination of Specimens From Patients With Carcinoma of the Stomach (Version: Stomach 4.2.0.0) [EB/OL]. Northfield: College of American Pathologists. Posting date: June 2021, accessing date: 1st March 2022. https://documents.cap.org/protocols/Stomach_4.2.0.0.REL_CAPCP.pdf
32. Liu S, Guan W, Wang H et al. (2014) Apparent diffusion coefficient value of gastric cancer by diffusion-weighted imaging: correlations with the histological differentiation and Lauren classification. Eur J Radiol 83:2122-2128. https://doi.org/10.1016/j.ejrad.2014.09.021.
33. Stocker D, Manoliu A, Becker AS et al. (2018) Image Quality and Geometric Distortion of Modern Diffusion-Weighted Imaging Sequences in Magnetic Resonance Imaging of the Prostate. Invest Radiol 53:200-206. https://doi.org/10.1097/RLI.0000000000000429.
34. Xu Y, Xu Q, Sun H et al. (2018) Could IVIM and ADC help in predicting the KRAS status in patients with rectal cancer? Eur Radiol 28:3059-3065. https://doi.org/10.1007/s00330-018-5329-y.
35. Lee EY, Yu X, Chu MM et al. (2014) Perfusion and diffusion characteristics of cervical cancer based on intraxovel incoherent motion MR imaging-a pilot study. Eur Radiol 24:1506-1513. https://doi.org/10.1007/s00330-014-3160-7.
36. Andreou A, Koh DM, Collins DJ et al. (2013)Measurement reproducibility of perfusion fraction and pseudodiffusion coefficient derived by intravoxel incoherent motion diffusion-weighted MR imaging in normal liver and metastases. Eur Radiol 23:428-434. https://doi.org/10.1007/s00330-012-2604-1.
37. Jerome NP, Miyazaki K, Collins DJ et al. (2017) Repeatability of derived parameters from histograms following non-Gaussian diffusion modelling of diffusion-weighted imaging in a paediatric oncological cohort. Eur Radiol 27:345-353. https://doi.org/10.1007/s00330-016-4318-2.
38. Li J, Wang Y, Wang R et al. (2022) Spectral CT for preoperative prediction of lymphovascular invasion in resectable gastric cancer: With external prospective validation. Front Oncol 12:942425. https://doi.org/10.3389/fonc.2022.942425.

39. Li J, Fang M, Wang R et al. (2018) Diagnostic accuracy of dual-energy CT-based nomograms to predict lymph node metastasis in gastric cancer. Eur Radiol 28:5241-5249. https://doi.org/10.1007/s00330-018-5483-2.